Harnessing Deformation to Switch On and Off the Propagation of Sound

*Sahab Babaee, Nicolas Viard, Pai Wang, Nicholas X. Fang, and Katia Bertoldi**

By combining numerical analyses and experiments we design a new class of architected materials to control the propagation of sound (also called acoustic metamaterials). The proposed system comprises an array of elastomeric helices in background air and is characterized by frequency ranges of strong wave attenuation (band gaps) in the undeformed configuration. Importantly, our results indicate that by axially stretching the helices, such band gaps can be suppressed, enabling the propagation of sound over all frequencies. The proposed concept expands the ability of existing acoustic metamaterials and paves the way for the design of a new class of materials and devices that enable better control and manipulation of sound.

Architected materials engineered to manipulate and control the propagation of sound have recently enabled the design of a range of novel acoustic devices.[1–9] In particular, the design of noise cancelling systems that take advantage of band gaps induced by both Bragg scattering[10–12] and local resonance[13–17] has been aggressively pursued. However, almost all of the proposed designs operate in fixed ranges of frequencies and their response cannot be tuned after their fabrication.[18] In an effort to design the next generation of acoustic tunable devices, it has been shown that the frequency range of the band gap can be modulated through application of mechanical deformation,[19] thermal radiation,[20] or rotation of the scatters.[21–25] However, different from the case of metamaterials designed to control the propagation of elastic[26–35] and electromagnetic[36–38] waves for which several strategies have been used to switch on and off the band gaps, the ability to turn on and off the propagation of sound over specific ranges of frequencies has not been extensively explored, and it has only been demonstrated through the rotation of the scatters.[21,23]

Here, we report a new class of acoustic metamaterials in which the applied deformation is exploited to switch on and off the propagation of sound over specific ranges of frequencies. The proposed structure comprises an array of elastomeric helices that can be easily stretched in the axial direction (see **Figure 1**). In the undeformed configuration the helices are in a compact state (see Figure 1a) and the system is equivalent to a square array of solid cylinders in air, which is known to be characterized by a complete band gap induced by Bragg scattering.[39] However, as the metamaterial is deformed, the pitch of the helices increases (see Figure 1b) and the air originally inside their internal cavity connects to the surrounding fluid, significantly reducing the solid volume fraction of the system. Importantly, we demonstrate that this change in volume fraction induced by the applied deformation is sufficient to suppress the initial band gap, giving us the opportunity to design a new class of acoustic switches.

We start by investigating the deformation of a single elastomeric helix. The helix is fabricated out of a silicone-based rubber[40] (vinyl polysiloxane with initial Young's modulus $E_0 = 784$ kPa, Poisson ratio $\nu_0 = 0.499$, and density $\rho = 965$ kg m^{-3}) via a molding approach (see Supporting Information for details). In the undeformed configuration it has diameter $D_0 = 28.6$ mm, pitch $P_0 = 13$ mm, and a rectangular cross-section of 13 mm × 6.5 mm. In **Figure 2**a we report experimental snapshots of a single helix at different levels of applied engineering strain, $\varepsilon = (H - H_0)/H_0 = 0, 0.40, 0.65$, and 0.90, where H_0 and H denote the undeformed and the deformed height of the helix, respectively. The experimental images are compared to the numerical snapshots obtained from non-linear finite element (FE) simulations (see Supporting Information for details) and clearly show that the pitch of the helix monotonically increases with the applied strain (note that the pitch varies along the length of the helix because of gravity), while its diameter remains almost unchanged. This can be explained by inspecting the parametric equations that describe the deformed helix

$$\mathrm{r}(\theta) = \left(\frac{D}{2}\cos\theta, \frac{D}{2}\sin\theta, \frac{P}{2\pi}\theta\right) \tag{1}$$

where the deformed pitch, P, and diameter, D, are given by (see Supporting Information for more details)

$$P = P_0(1+\epsilon),\ D = \sqrt{D_0^2 - \frac{P_0^2}{\pi^2}\,\epsilon\,(\epsilon+2)} \tag{2}$$

In Figure 2b,c, we report the evolution of P and D as a function of the applied strain ε, as predicted by Equation (2) (red dashed lines). The analytical results indicate that, while the change in diameter is limited to 3% for $\varepsilon = 0.9$, the pitch length almost doubles (i.e., $P/P_0 = 1.9$ at $\varepsilon = 0.9$). Finally, we note that in Figure 2b,c the analytical predictions are also compared to both the experimental (green markers) and FE (blue markers) results, showing an excellent agreement and therefore validating our simple geometric model.

S. Babaee, P. Wang, Prof. K. Bertoldi
Harvard John A. Paulson School of Engineering and Applied Sciences
Harvard University
Cambridge, MA 02138, USA
E-mail: bertoldi@seas.harvard.edu
Dr. N. Viard, Prof. N. X. Fang
Department of Mechanical Engineering
Massachusetts Institute of Technology
Cambridge, MA 02139, USA
Prof. K. Bertoldi
Kavli Institute
Harvard University
Cambridge, MA 02138, USA

DOI: 10.1002/adma.201504469

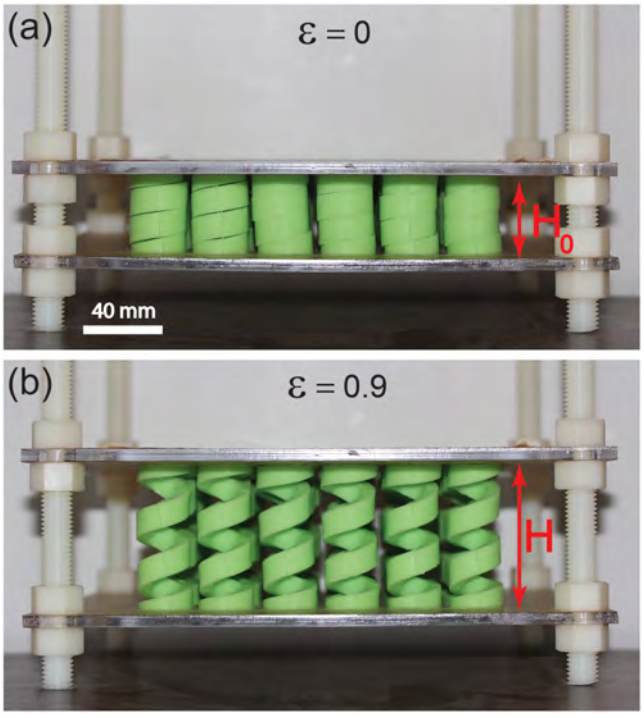

Figure 1. Acoustic switch. The fabricated acoustic switch comprises a 6 × 6 square array of stretchable helices. a) In the undeformed configuration (i.e., $\varepsilon = 0.0$), the helices are in a compact state and can be regarded as solid cylinders of height $H_0 = 40$ mm. As a result, the metamaterial is characterized by a frequency range of strong wave attenuation (band gap). b) As the helices are stretched, the solid volume fraction of the metamaterial drops significantly and the band gap is suppressed.

Focusing on a metamaterial comprising a square array of helices with center-to-center distance A_0 = 32.5 mm, it is easy to see that the large change in pitch induced by the applied strain significantly alters the solid volume fraction of the system. In fact, since here we focus on acoustic waves propagating in the surrounding air, in the undeformed configuration each helix can be considered as a solid cylinder (as the air inside the cavities of the hollow cylinders is not connected to the outside surrounding air) and the solid volume fraction of the metamaterial can be calculated as $\psi_0 = \pi D_0^2/(4A_0^2) = 0.61$. However, as the metamaterial is stretched, the cylinders transform into helices and the air originally inside their internal cavity connects to the surrounding fluid, reducing the solid volume fraction. In particular, for $\varepsilon > 0$ the solid volume fraction can be simply obtained as (see Supporting Information for details)

$$\psi = \frac{\pi(D_0^2 - D_{0,\text{in}}^2)}{4A_0^2(\epsilon + 1)}, \tag{3}$$

where $D_{0,\text{in}} = 15.6$ mm denotes the inner diameter of the helices and we have made use of the fact that the volume of the elastomeric helices is preserved during deformation. In Figure 2d we report the evolution of ψ as a function of ε. The results indicate that at first, as the helices are slightly stretched, ψ immediately reduces from 0.61 to 0.41 and then gradually decreases to reach 0.22 as ε rises to 0.9. Importantly, we expect this change in ψ to have a profound impact on the propagation of sound, as it is well known that the size of the acoustic band gap for an acoustic metamaterial significantly depends on the solid volume fraction.[41]

Next, we numerically investigate the propagation of sound waves through the acoustic metamaterial at different levels of applied deformation. For this set of simulations we assume the metamaterial to be infinite and use a prismatic unit cell of size $A_0 \times A_0 \times P_0$ in the undeformed configuration. The analysis consists of two steps: (i) we first build a 3D model of the helix (comprising only one loop), mesh it using solid element (Abaqus element type C3D10M with seed size of 1 mm), apply periodic boundary conditions along the axial direction, and deform it by applying a strain ε; (ii) we then change the elements of the deformed helix into acoustic elements (Abaqus element type AC3D10M), mesh also the surrounding air in the unit cell using the same type of elements (for the air we assume density $\rho_{\text{air}} = 1.2$ kg m^{-3} and speed of sound c_{air} = 343 m s^{-1}), and finally calculate the dispersion relation by using frequency domain analyses (see Supporting Information for more details). Note that, since in this study we only focus on waves propagating in the plane perpendicular to the axis of the helices, the dispersion diagrams are constructed considering wave vectors lying in that plane.

In **Figure 3**a,b we show the dispersion relations calculated for the undeformed ($\varepsilon = 0$; Figure 3a) and highly deformed ($\varepsilon = 0.9$; Figure 3b) metamaterials. At ε = 0, a wide complete band gap is found at f = 4.64–7.28 kHz (highlighted as the blue-shaded area in Figure 3a), so that sound waves within this frequency range are not expected to propagate through the system. However, as the deformation is progressively increased, this band gap is found to monotonically reduce its width (see Figures S5 and S6, Supporting Information), and at $\varepsilon = 0.9$ it is fully closed (Figure 3b).

To confirm the numerical predictions, we experimentally test the dynamic response in GX direction of an acoustic metamaterial consisting of 36 stretchable helices arranged in a 6 × 6 square lattice with the center-to-center distance, A_0 = 32.5 mm. In order to stretch all the helices simultaneously and to immobilize them at the strain level of interest, we use a fixture made of acrylic plates and nylon bolts/nuts (see Figure 1). Moreover, 2 inch thick closed-cell foam plates are placed all around the sample to acoustically insulate it from the spurious reflections and create homogeneous boundaries all around the sample (see Figure S2, Supporting Information). Acoustic waves through air are then excited by an array of five identical loudspeakers (Vifa OT19NC00-04, 3/4 in. diameter) placed along one face of the sample and the amplitude of the scattered pressure waves is recorded by a microphone and preamplifier (model 378B02, PCB Piezotronics) mounted on the opposite face. Note that the propagation of sound in air through the acrylic plates surrounded by foams without the helices is also recorded and that, to reduce the effect of boundaries, the normalized transmission spectrum is computed as $20\log_{10}||\hat{\phi}(f)/\hat{\phi}_{\text{air}}(f)||$, where $\hat{\phi}(f)$ and $\hat{\phi}_{\text{air}}(f)$ are the Fourier transforms of the transmission through the sample and air, respectively (see Supporting Information for details). Finally, it is important to point out that in order to minimize the effect of sound waves propagating along the axial direction of the helices and to better approximate the conditions considered in our numerical simulations (where we only

Adv. Mater. 2015,
DOI: 10.1002/adma.201504469

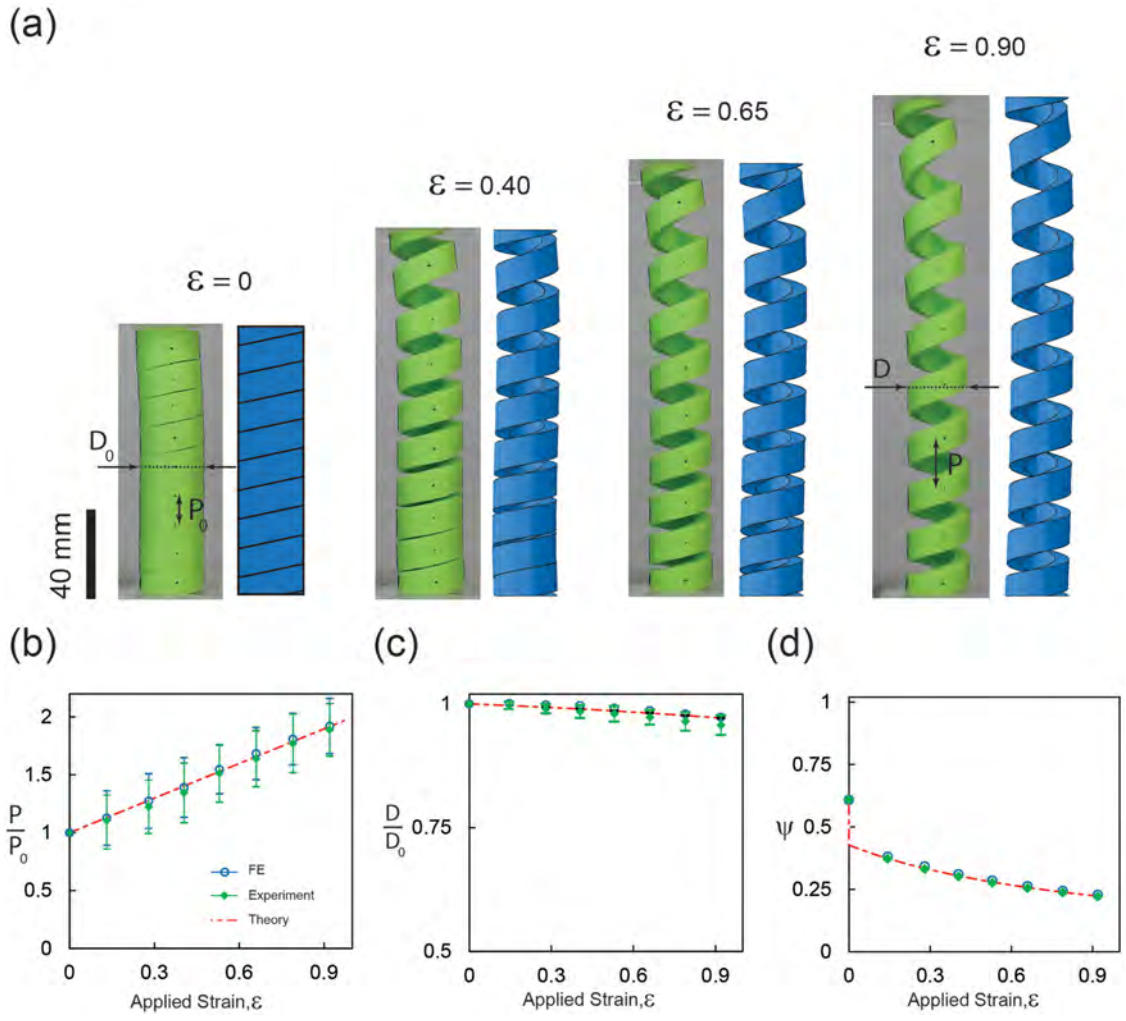

Figure 2. Deformation of the helices. a) Experimental (green samples) and numerical (blue models) images of a single helix at different levels of applied strain, $\varepsilon = 0, 0.40, 0.65,$ and 0.90. P_0 and D_0 are the pitch length and outer diameter of the helix, respectively, at $\varepsilon = 0$. Evolution of b) pitch length, P, c) outer diameter, D, and d) solid volume fraction, ψ, as a function of the applied strain. Analytical predictions (red dashed line) are compared to both experimental (green markers) and numerical (blue markers) results.

take into account waves propagating in the plane perpendicular to the axis of the helices), the initial height of the metamaterial ($H_0 = 40$ mm) is chosen to be approximately equal to the minimum wavelength of excitation during the experiment (38 mm at 9 kHz).

The transmission spectra of sound waves through the sample, measured at $\varepsilon = 0$ and 0.9, are reported as green lines in Figure 3c,d, respectively. In the undeformed configuration, we find that the transmission is characterized by a drop of ≈30 dB for $f = 2.75$–7.40 kHz (Figure 3c), in close agreement with the numerical results for the corresponding infinite structure. In fact, the dispersion relation for the undeformed system reported in Figure 3a not only indicates the presence of a complete (i.e., for all directions) band gap for $f = 4.64$–7.28 kHz, but also shows that in GX direction the frequency range of strong wave attenuation is significantly wider ($f = 2.90$–7.28 kHz). Differently, for $\varepsilon = 0.9$ the acoustic waves with frequency in the range $f = 2.75$–7.40 kHz are found to propagate through the material (i.e., the transmission fluctuates around 0 for this range of frequency; see Figure 3d), confirming that the proposed metamaterial can be utilized as an acoustic switch whose response is controlled by the applied deformation. Finally, we also note that in the highly stretched structure ($\varepsilon = 0.9$) a drop of ≈20 dB in transmission is found at $f = 8$–9 KHz (Figure 3d), in correspondence of the band gap in GX direction at $f = 7.55$–9.00 kHz observed in the corresponding dispersion relation (see Figure 3b).

Having demonstrated that the applied deformation can be exploited to design acoustic switches, we now show that the response of the system is robust. To this end, we numerically investigate the effect of both arrangement of the helices and their geometry on propagation of sound. In **Figure 4**a we report the evolution of the band gaps frequencies as a function of the applied strain for a triangular arrangement of the helices with the same geometry as those shown in Figure 1 (i.e., $D_0 = 28.6$ mm, $P_0 = 13$ mm and rectangular cross-section of 13 mm × 6.5 mm). For a triangular array with center-to-center distance $A_0 = 32.5$ mm, we find a complete band

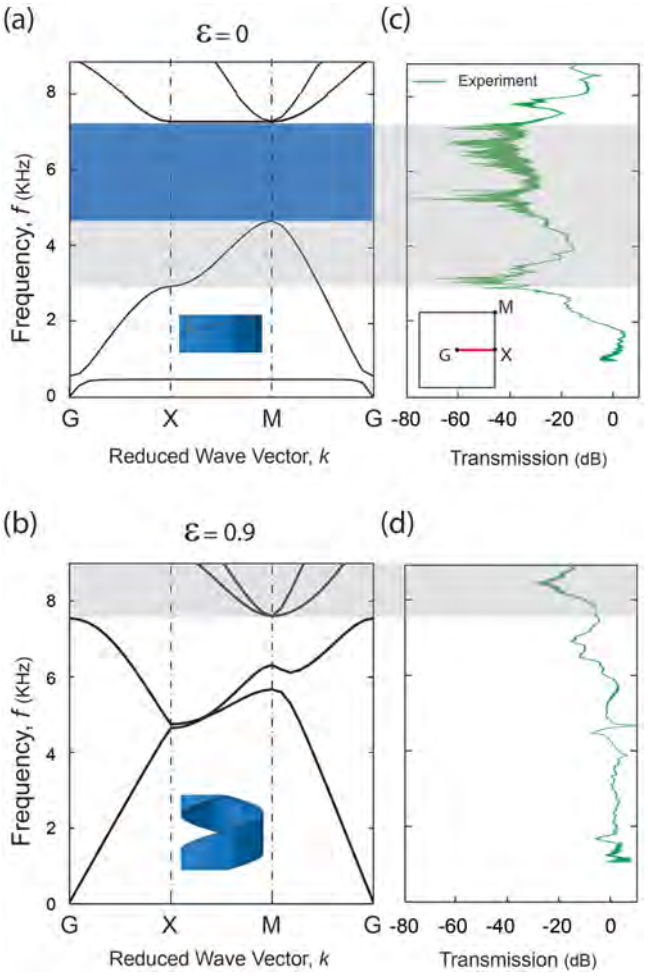

Figure 3. Propagation of sound through the metamaterial at different levels of applied deformation. a,b) Dispersion relations and c,d) experimentally measured transmission spectra for acoustic waves propagating along the GX direction. Results are shown for (a,c) the undeformed configuration ($\varepsilon = 0$) and (b,d) the stretched configuration ($\varepsilon = 0.9$).

gap at f = 9.0–10.5 kHz in the undeformed configuration (ε = 0.0). Importantly, this gap can be completely suppressed by stretching the system by $\varepsilon = 1.3$ (see Figure S8 in Supporting Information for details). We also note that the discontinuity of the band gap frequency found at small values of applied strain (i.e., $\varepsilon \to 0$) is due to the sudden drop in solid volume fraction (from 0.70 to 0.49) that takes place when the metamaterial is slightly stretched. Furthermore, we also systematically investigate the effect of the geometry of the helices on the dynamic response of the resulting metamaterial. In particular, we focus on helices with outer diameter $D_0 = 28.6$ mm arranged to form a square lattice with center-to-center spacing $A_0 = 32.5$ mm and perform a series of simulations where we change their cross-sectional thickness ($t = (D_0 - D_{0,in})/2$) and height ($h = P_0$). The results of this parametric study (reported as a contour map in Figure 4b) demonstrate that we have identified a robust and efficient strategy to switch on and off the propagation of sound. In fact, we find not only that the applied deformation can be harnessed to switch on and off the propagation of sound for all considered configurations, but also that by changing the geometry of the helices the amount of strain needed to fully suppress the band gaps can be tuned. In particular, helices with $t = 1.6$ mm and $h = 3.2$ mm are observed to require the lowest applied strain, $\varepsilon \approx 0.2$, to suppress the band gap, while, irrespectively of h, helices with $t = 14.3$ mm result in the highest value of strain, $\varepsilon \approx 1.1$, to fully suppress the band gap (see Figure 4b and Figure S7, Supporting Information).

In summary, we demonstrated both numerically and experimentally that deformation in periodic arrays of helices can be intentionally exploited to switch on and off the propagation of the sound. Our results indicate that externally applied tension provides a simple mechanism to significantly alter the solid volume fraction of the system and, consequently, achieve a wide range of tunability for the band gap. Importantly, the transformation of the band gaps is fully reversible and the range of frequencies affected by the applied deformation can be tuned

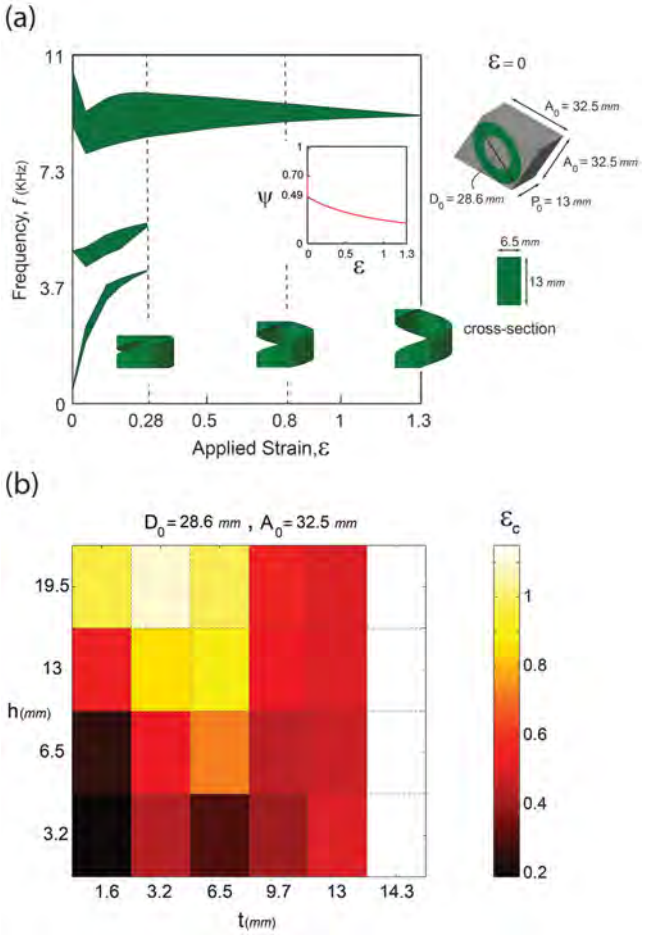

Figure 4. Effect of arrangement of the helices and their geometry. a) Evolution of the band gap frequency, f, as a function of the applied strain, ε, for a triangular array (with lattice spacing A_0 = 32.5 mm) of helices with initial outer diameter $D_0 = 28.6$ mm, pitch $P_0 = 13$ mm, and rectangular cross-section of 13 × 6.5 mm. The inset shows the evolution of the solid volume fraction as a function of the applied strain. b) Effect of the cross-section dimensions $h = P_0$ and $t = (D_0 - D_{0,in})/2$ on the amount of strain needed to fully suppress the band gaps (ε_c) for a square array of helices with fixed initial outer diameter $D_0 = 28.6$ mm and lattice spacing $A_0 = 32.5$ mm.

Adv. Mater. 2015,
DOI: 10.1002/adma.201504469

by varying the geometry of the helices. Moreover, although in this study we only demonstrated the concept for an array of vertical helices at the centimeter scale, the proposed design can be applied to more complex arrangements of helices and various length scales, enabling the design of materials and devices to control the propagation of ultrasound (in the case of microscale systems) and intrasound (in the case of macroscale systems) along arbitrary directions. From a practical perspective, the full active control over the propagation of sound in combination with the wealth of different length scales and geometrical designs provides a new class of architected materials with a broad field of applications ranging from switchable wave guides to tunable imaging devices.

Supporting Information

Supporting Information is available from the Wiley Online Library or from the author.

Acknowledgements

This work was supported by NSF through grant CMMI-1120724. K.B. acknowledges support by Harvard MRSEC through grant DMR-1420570 and NSF through grant CMMI-1149456 (CAREER). N.X.F. acknowledges the financial support by Office of Naval Research, Multidisciplinary University Research Initiative, Grant No. N00014-13-1-0631. The authors are also grateful to Dr. Farhad Javid, Johannes Overvelde, Dr. Jun Xu, Kai Xu, and Dr. Andrew Gross for inspirational discussions and help.

Received: September 11, 2015
Revised: October 16, 2015
Published online:

[1] L. Zigoneanu, Bi. Popa, S. A. Cummer, *Nat. Mater.* **2014**, *13*, 1.
[2] B. Liang, X. S. Guo, J. Tu, D. Zhang, J. C. Cheng, *Nat. Mater.* **2010**, *9*, 989.
[3] M. Maldovan, *Nature* **2013**, *503*, 209.
[4] N. Fang, D. Xi, J. Xu, M. Ambati, W. Srituravanich, C. Sun, X. Zhang, *Nat. Mater.* **2006**, *5*, 452.
[5] M. H. Lu, C. Zhang, L. Feng, J. Zhao, Y. F. Chen, Y. W. Mao, J. Zi, Y. Y. Zhu, S. N. Zhu, N. B. Ming, *Nat. Mater.* **2007**, *6*, 744.
[6] J. Shi, D. Ahmed, X. Mao, S. S. Lin, A. Lawit, T. J. Huang, *Lab Chip* **2009**, *9*, 2890.
[7] A. Climente, D. Torrent, J. Sánchez-Dehesa, *Appl. Phys. Lett.* **2012**, *100*, 144103, .
[8] A. Climente, D. Torrent, J. Sánchez-Dehesa, *Appl. Phys. Lett.* **2010**, *97*, 104103.
[9] L. Sanchis, V. M. Garcia-Chocano, R. Llopis-Pontiveros, A. Climente, R. Martinez-Pastor, F. Cervera, J. Sánchez-Dehesa, *Phys. Rev. Lett.* **2013**, *110*, 124301.
[10] M. H. Lu, L. Feng, Y. F. Chen, *Mater. Today* **2009**, *12*, 34.
[11] N. Sui, X. Yan, T. Y. Huang, J. Xu, F. G. Yuan, Y. Jing, *Appl. Phys. Lett.* **2015**, *106*, 171905.
[12] J. Sánchez-Dehesa, V. M. Garcia-Chocano, D. Torrent, F. Cervera, S. Cabrera, *J. Acoust. Soc. Am.* **2011**, *129*, 1173.
[13] G. Ma, M. Yang, S. Xiao, Z. Yang, P. Sheng, *Nat. Mater.* **2014**, *13*, 873.
[14] J. Mei, G. Ma, M. Yang, Z. Yang, W. Wen, P. Sheng, *Nat. Commun.* **2012**, *3*, 756.
[15] Z. Liang, M. Willatzen, J. Li, J. Christensen, *Sci. Rep.* **2012**, *2*, 859.
[16] B. M. Assouar, M. Senesi, M. Oudich, M. Ruzzene, Z. Hou, *Appl. Phys. Lett.* **2012**, *101*, 173505.
[17] Z. Yang, H. M. Dai, N. H. Chan, G. C. Ma, P. Sheng, *Appl. Phys. Lett.* **2010**, *96*, 041906.
[18] O. B. Matar, J. Vasseur, (Ed. P. A. Deymier), *Acoustic Metamaterials and Phononic Crystals*, Springer-Verlag, Berlin; Heidelberg, Germany, **2013**.
[19] Y. Huang, W. Q. Chen, Y. S. Wang, W. Yang, *AIP Adv.* **2015**, *5*, 027138.
[20] E. Walker, D. Reyes, M. M. Rojas, A. Krokhin, Z. Wang, A. Neogi, *Appl. Phys. Lett.* **2014**, *105*, 143503.
[21] C. Goffaux, J. Vigneron, *Phys. Rev. B* **2001**, *64*, 075118.
[22] V. Romero-García, C. Lagarrigue, J. P. Groby, O. Richoux, V. Tournat, *J. Physics D: Appl. Phys.* **2013**, *46*, 305108.
[23] F. Wu, Z. Liu, Y. Liu, *Phys. Rev. E* **2002**, *66*, 046628.
[24] X. F. Li, X. Ni, L. Feng, M. H. Lu, C. He, Y. F. Chen, *Phys. Rev. Lett.* **2011**, *106*, 084301, .
[25] S. C. S. Lin, T. J. Huang, *Phys. Rev. B* **2011**, *83*, 174303.
[26] L. Airoldi, M. Ruzzene, *New J. Phys.* **2011**, *13*, 113010.
[27] A. Bergamini, T. Delpero, L. D. Simoni, L. D. Lillo, M. Ruzzene, P. Ermanni, *Adv. Mater.* **2014**, *26*, 1343.
[28] M. Gei, S. Roccabianca, *IEEE/ASME Trans. Metatron.* **2011**, *16*, 102.
[29] N. Boechler, J. Yang, G. Theocharis, P. G. Kevrekidis, C. Daraio, *J. Appl. Phys.* **2011**, *109*, 074906.
[30] S. Rudykh, M. C. Boyce, *Phys. Rev. Lett.* **2014**, *112*, 034301.
[31] Y. Wang, F. Li, Y. Wang, K. Kishimoto, W. Huang, *Acta Mech. Sin.* **2009**, *25*, 65.
[32] S. Babaee, P. Wang, K. Bertoldi, *J. Appl. Phys.* **2015**, *117*, 244903.
[33] P. Wang, F. Casadei, S. Shan, J. C. Weaver, K. Bertoldi, *Phys. Rev. Lett.* **2014**, *113*, 014301.
[34] D. Mousanezhad, S. Babaee, R. Ghosh, E. Mahdi, K. Bertoldi, A. Vaziri, *Phys. Rev.B* **2015**, *92*, 104304.
[35] K. Bertoldi, P. Wang, S. Shan, S. Babaee, *J. Acoust. Soc. Am.* **2014**, *135*, 2254.
[36] J. H. Lee, C. Y. Koh, J. P. Singer, S. J. Jeon, M. Maldovan, O. Stein, E. L. Thomas, *Adv. Mater.* **2014**, *26*, 532.
[37] X. Mao, S. S. Lin, M. I. Lapsley, J. Shi, B. K. Juluri, T. J. Huang, *Lab Chip* **2009**, *9*, 2050.
[38] C. Y. Liu, L. W. Chen, *Phys. Rev. B* **2005**, *72*, 1.
[39] J. V. Sánchez-Pérez, D. Caballero, R. Martinez-Sala, C. Rubio, J. Sanchez-Dehesa, F. Meseguer, J. Llinares, F. Galvez, *Phys. Rev. Lett.* **1998**, *80*, 5325.
[40] S. Babaee, J. Shim, J. C. Weaver, E. R. Chen, N. Patel, K. Bertoldi, *Adv. Mater.* **2013**, *25*, 5044.
[41] M. Maldovan, E. L. Thomas, *Periodic Materials and Interference Lithography: for Photonics, Phononics and Mechanics*, Wiley-VCH, Weinheim, Germany, **2009**.

ADVANCED MATERIALS

Supporting Information

for *Adv. Mater.*, DOI: 10.1002/adma.201504469

Harnessing Deformation to Switch On and Off the Propagation of Sound

*Sahab Babaee, Nicolas Viard, Pai Wang, Nicholas X. Fang, and Katia Bertoldi**

Supporting Information
Harnessing deformation to switch on and off the propagation of sound

Sahab Babaee[1], Nicolas Viard[2], Pai Wang[1], Nicholas X. Fang[2], and Katia Bertoldi[1,3]

[1]*Harvard John A. Paulson School of Engineering and Applied Sciences, Harvard University, Cambridge, MA 02138*
[2]*Department of Mechanical Engineering, Massachusetts Institute of Technology, Cambridge, MA 02139*
[3]*Kavli Institute, Harvard University, Cambridge, MA 02138*

S1 Fabrication

A silicone-based rubber (commercial name: Elite Double 32, *Zhermack*) with material density $\rho = 965\,kg/m^3$ is used to cast the experimental specimen. The material properties are measured through tensile testing up to a true strain of 0.60 and no hysteresis is found during loading and unloading. The constitute behavior is accurately captured by a nearly-incompressible (i.e. Poisson ratio $\nu_0 = 0.4999$) Yeoh hyperelastic model [1], whose strain energy is given by

$$W = \sum_{i=1}^{3} C_{i0} \left(\bar{I}_1 - 3\right)^i + \frac{(J-1)^{2i}}{D_i}, \tag{S1}$$

where $C_{10} = 131\,kPa, C_{20} = 0\,kPa, C_{30} = 3.5\,kPa, D_1 = D_2 = D_3 = 1.54\,GPa^{-1}$. Moreover, $\bar{I}_1 = \text{tr}\left[\text{dev}\left(\mathbf{F}^T\mathbf{F}\right)\right]$ and $J = \det\mathbf{F}$, where $\mathbf{F}$ is the deformation gradient. Note that the initial shear modulus(G_0) and bulk modulus(K_0) at zero strain are related to two of the Yeoh model parameters as $G_0 = 2\,C_{10} = 0.26\,MPa, K_0 = 2/D_1 = 1.3\,GPa$, so that the speed of propagating longitudinal waves through the undeformed homogeneous rubber is $c_L = 1160\,m/s$.

To manufacture the helices a molding approach is used. First, a mold is fabricated from Rigid Opaque Vero blue plastic material (product number RGD840, *Objet*) using a 3-D printer (Connex500, *Objet*) to cast a helix (see Figure S1(a)). Before replication, a releasing agent (*SMOOTH-ON* universal mold release) is sprayed on to the mold to easily de-mold and separate the cured rubber helix from the plastic mold. The casted mixture is first placed in vacuum for degassing and is allowed to set at room temperature for curing. The single helices fabricated to study their static response (i.e. deformation) are comprised of 9.2 loops (both ends are cut flat - see Figure S1(b)) with rectangular cross-section of $13\,mm \times 6.5\,mm$, inner diameter $D_{0,in} = 15.6\,mm$, outer diameter $D_0 = 28.6\,mm$, and pitch $P_0 = 16.25\,mm$.

To fabricate the acoustic metamaterial shown in Figure 1 of the main text, we manufacture 36 elastomeric helices and arrange them to form a 6×6 two-dimensional square lattice with center-to-center distance $A_0 = 32.5\,mm$. Note that all helices are cut to comprise only 3 loops (so that their height in the undeformed configuration is $H_0 = 40$ mm) before building the specimen. The helices are then attached to two acrylic plates on the top and bottom using *Cyberbond* Apollo 2240 adhesive. We use four nylon bolts/nuts placed at the corners of the plates to immobilize the specimen at strain level of interest (Figure S2(a)). The dimension of the specimen at $\epsilon = 0$ (i.e. undeformed configuration) is Height $\times$ Width $\times$ Depth $= 40 \times 195 \times 195\ mm$.

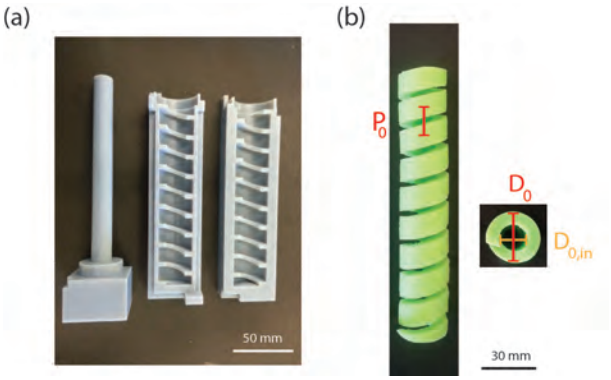

Figure S1: **Fabrication.** (a) 3-D printed plastic mold, and (b) elastomeric helix manufactured using the mold and casting approach.

S2 Testing

We measure the propagation of sound waves through the metamaterial at two levels of applied deformation, $\epsilon = 0$ and $\epsilon = 0.9$. At the strain level of interest, we immobilize the specimen using the acrylic fixture and measure the transmission in GX direction. In all the tests we also place a 2 inch-thick closed-cell foams all around the sample to properly close it regardless of its height (Figure S2(c)). To excite the wave propagation through the air, we use an array of five identical loudspeakers (Vifa OT19NC00-04, 3/4 inch diameter)(Figure S2(b)) placed along one of the faces of the sample. The loudspeakers provide a frequency sweep input signal (duration 1 second), whose frequency content is controlled with a MATLAB script (spanning from 500 Hz to 12 kHz). On the opposite face of the sample we then record the amplitude of the scattered pressure waves, $\phi(t)$, with a PCB microphone and pre-amplifier (model 378B02, PCB). Note that the transmission in air, $\phi_{air}(t)$, through the acrylic plates surrounded by foams without the helices, is also recorded. Finally, the normalized transmission spectra reported in Figure 3 in the main text are calculated as

$$T(f) = 20 \log_{10} \left(\left\| \frac{\hat{\phi}(f)}{\hat{\phi}_{air}(f)} \right\| \right)$$

where $\hat{\phi}(f)$ and $\hat{\phi}_{air}(f)$ are the Fourier transforms of the transmission through the sample and the transmission through air, respectively. Note that each curve shown in Figure 3 is based on the average of 20 measurements.

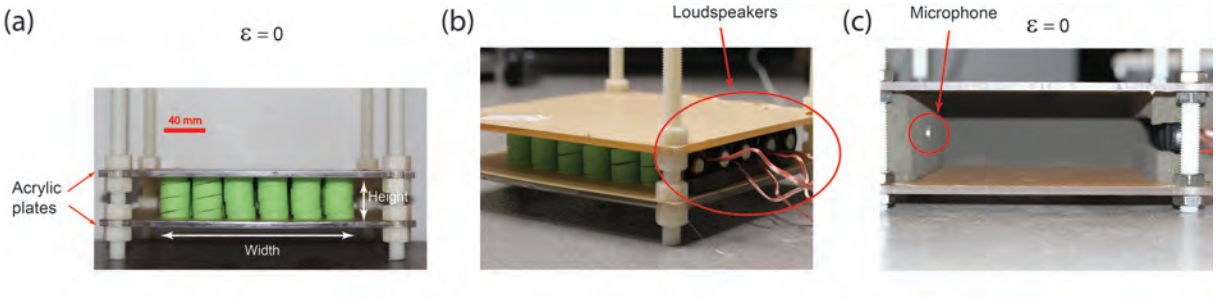

Figure S2: **Testing.** (a) Front-view image of the fabricated metamaterial at $\epsilon = 0$. (b) Position of loudspeakers in the experimental set-up. (c) Experimental set-up without the metamaterial used to measure the transmission through air.

S3 Analytical model for the deformation of an helix

In this Section we present a simple analytical model to predict the effect of the applied strain, ϵ, on the morphology of a helix. In particular, we first investigate how ϵ affects its pitch P and outer diameter D, and then determine the effect of such deformation on the solid volume fraction ψ of the metamaterial.

We start by noting that the deformed configuration of the helix is described by the vector function

$$\mathbf{r}(\theta) = (x(\theta),\, y(\theta),\, z(\theta)) = \left(\frac{D}{2} \cos\theta,\, \frac{D}{2} \sin\theta,\, \frac{P}{2\pi}\theta \right). \tag{S2}$$

Assuming P_0 the pitch of an helix composed of N loops in the undeformed configuration (i.e. at $\epsilon = 0$), it is easy to see that at $\epsilon = 0$ the height of the helix is given by

$$H_0 = N\,P_0, \tag{S3}$$

while under an applied strain ϵ we have

$$H(\epsilon) = N\,P = (1+\epsilon)\;H_0. \tag{S4}$$

Note that for the sake of simplicity, we have assumed that the pitch remains constant along the helix, a condition that is violated in the presence of gravity. Substitution of Eq. (S3) into Eq. (S4) yields the evolution of the pitch as a function of the applied strain

$$P = (1+\epsilon)P_0. \tag{S5}$$

To obtain the diameter of the helix in the deformed configuration (D), we first calculate the length of one loop of the helix both in the deformed configuration

$$L = \int_0^{2\pi} \sqrt{\left(\frac{\mathrm{d}x}{\mathrm{d}\theta}\right)^2 + \left(\frac{\mathrm{d}y}{\mathrm{d}\theta}\right)^2 + \left(\frac{\mathrm{d}z}{\mathrm{d}\theta}\right)^2}\;\mathrm{d}\theta = \sqrt{\pi^2 D^2 + P^2}, \tag{S6}$$

and in the undeformed configuration

$$L_0 = \sqrt{\pi^2 D_0^2 + P_0^2}. \tag{S7}$$

Next, we assume that the helix is inextensible (i.e. $L = L_0$), so that

$$\sqrt{\pi^2 D_0^2 + P_0^2} = \sqrt{\pi^2 D^2 + P^2}, \tag{S8}$$

from which D is obtained as

$$D = D_0\sqrt{1 - \left(\frac{P_0}{\pi D_0}\right)^2 \epsilon\,(\epsilon+2)}. \tag{S9}$$

In particular, for the helix manufactured for this study (characterized by $P_0 = 13\ mm$ and $D_0 = 28.6\ mm$) we have

$$D = 28.6\sqrt{1 - 0.021\,\epsilon\,(\epsilon+2)}\,mm. \tag{S10}$$

Finally, we focus on the metamaterial and consider a square array of helices with center-to-center distance $A_0 = 32.5$ mm. It is easy to see that the change in pitch induced by the applied strain significantly alters the solid volume fraction of the system. Since in this study we focus on pressure waves propagating in the air surrounding the helices, in the undeformed configuration each helix can be considered as a solid cylinder and the solid volume fraction of the metamaterial can be obtained as

$$\psi_0 = \frac{V_{cylinder}}{V_{unit\,cell}} = \frac{\pi D_0^2}{4A_0^2}. \tag{S11}$$

However, as the applied deformation is increased, the cylinders transform into helices and the air originally inside their internal cavity connects to the surrounding fluid, reducing the solid

volume fraction of the metamaterial. Therefore, for $\epsilon > 0$ the solid volume fraction can be calculated as

$$\psi = \frac{V_{helix}}{V_{unit\,cell}} = \frac{V_{helix}}{A_0^2 H_0(1+\epsilon)}. \tag{S12}$$

Since the helices are made of an incompressible material (rubber), their volume is preserved during deformation and can be easily calculated as

$$V_{helix} = \frac{\pi}{4}(D_0^2 - D_{0,in}^2)\ H_0, \tag{S13}$$

where $D_{0,in}$ is the inner diameter of the helix in the undeformed configuration (i.e. at $\epsilon = 0$). Thus, the solid volume fraction of the metamaterial under an applied strain ϵ is simply given by

$$\psi = \frac{\pi(D_0^2 - D_{0,in}^2)}{4A_0^2\ (1+\epsilon)}. \tag{S14}$$

S4 Numerical Simulations

All the numerical simulations are carried out using the commercial Finite Element package Abaqus/Standard (SIMULIA, Providence, RI). In particular we conduct two different types of simulations: (*i*) static analysis to investigate the effect of the applied deformation on the shape of the helix; (*ii*) Bloch wave analysis to investigate the propagation of small-amplitude acoustic waves in the metamaterial under different levels of deformation.

S4.1 Static analysis

Static analyses are performed to capture the deformed configuration of the helices under an applied strain ϵ, accounting for the effect of gravity. The FE model of a single helix with the same geometric and material properties as the fabricated one is constructed using quadratic solid elements (Abaqus element type C3D10M with a mesh seed size of 1 mm). Moreover, the response of the material is captured using the Yeoh hyperelastic model described in Section S1. In the simulations we apply a vertical displacement $u = \epsilon H_0$ to the top face of the helix, while constraining the motion of the bottom face. We then monitor the effect of the applied deformation on the pitch and outer diameter. Snapshots of the meshed undeformed and deformed (at $\epsilon = 0.9$) helix are shown in Figure S3.

S4.2 Bloch wave analysis

The propagation of sound waves within the acoustic metamaterial is first investigated numerically by considering a square array of helices of infinite extent, characterized by a prismatic unit cell (i.e. minimum unit identified in the periodic structure which includes both the helix and the surrounding air) spanned by the lattice vectors $\mathbf{a}_1 = [A_0,\, 0,\, 0]$, $\mathbf{a}_2 = [0,\, A_0,\, 0]$, and $\mathbf{a}_3 = [0,\, 0,\, P]$, as shown in Figure S4(b). Thus, any spatial function field, $\phi(\mathbf{x})$, in the infinite periodic structure satisfies the condition:

$$\phi(\mathbf{x} + \mathbf{T}) = \phi(\mathbf{x}), \tag{S15}$$

where

$$\mathbf{T} = t_1\mathbf{a}_1 + t_2\mathbf{a}_2 + t_3\mathbf{a}_3, \tag{S16}$$

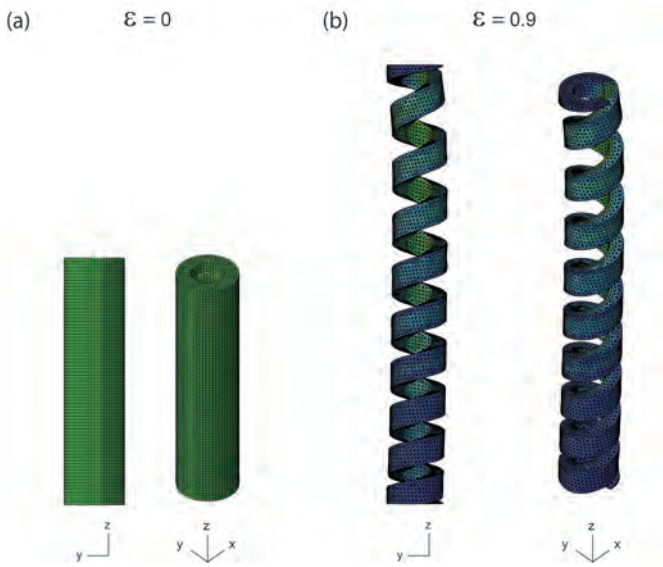

Figure S3: **Numerical images of a single helix.** Front and isometric views of (a) the undeformed and (b) highly deformed (i.e. $\epsilon = 0.9$) configuration as obtained from the static analysis.

t_1, t_2, and t_3 being arbitrary integers.

The analysis to obtain the dispersion relation of the propagating waves in the periodic structure at different levels of applied deformation consists of two steps: (**Step 1**) we apply statically the desired level of deformation to the unit cell; (**Step 2**) we calculate the dispersion relation of the propagating waves for the deformed unit cell.

Step 1. We mesh the unit cell (comprising only one loop of the helix) using quadratic solid element (Abaqus element type C3D10M) and applied statically the desired level of deformation. To this end, we apply periodic boundary conditions along the axial direction, so that the displacements of each pair of nodes periodically located on the top and bottom faces of the unit cell are related as

$$u_x^t - u_x^b = 0, \qquad u_y^t - u_y^b = 0, \qquad u_z^t - u_z^b = \epsilon(Z^t - Z^b), \tag{S17}$$

where the superscripts t and b refer to quantities associated to nodes on the top and bottom surfaces and Z denotes the position in z-direction of a node in the undeformed configuration. Then, a non-linear static step is performed to deform the unit cell by applying the desired value of strain ϵ.

Step 2. We investigate the dynamic response of the metamaterial and conduct frequency domain wave propagation analysis on the deformed the unit cell at different levels of applied deformation, focusing on the propagation of waves in the xy-plane. In particular, we change the elements of the deformed unit cell obtained through Step 1 into acoustic elements (Abaqus element type AC3D10M), and mesh also the surrounding air in the unit cell using the same type of elements (for the air we assume density $\rho_{air} = 1.2\, kg/m^3$ and speed of sound $c_{L,air} = 343\, m/s$).

Next, we apply to the faces of the deformed unit cell Bloch-type boundary conditions of the form

$$\mathrm{p}(\mathbf{x} + \mathbf{r}) = \mathrm{p}(\mathbf{x}) \exp(i\mathbf{k} \cdot \mathbf{r}), \tag{S18}$$

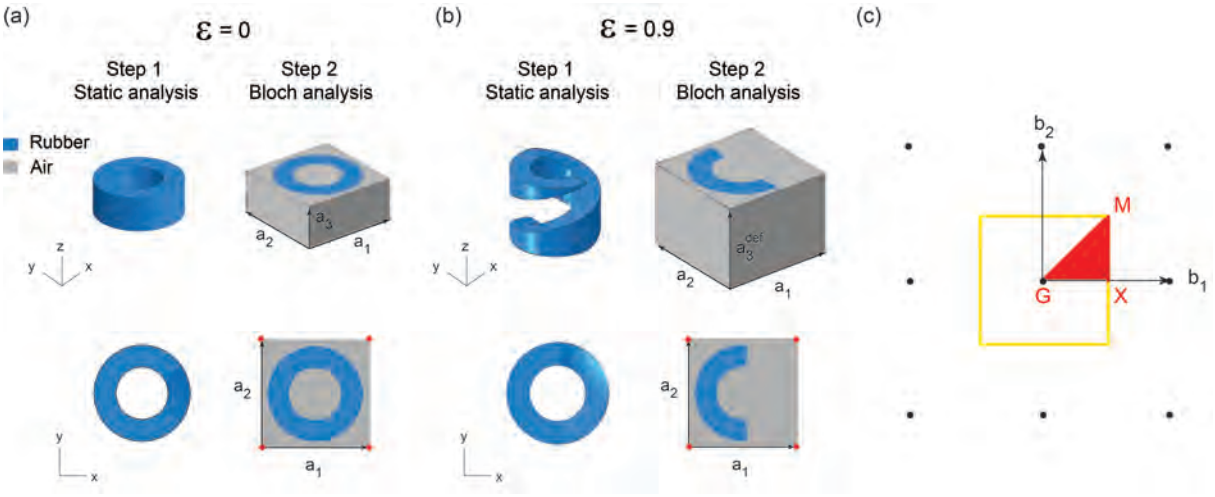

Figure S4: **Bloch wave analysis.** (a) Undeformed configuration ($\epsilon = 0$): oblique and top views of the unit cell as obtained from Step 1 (static analysis) and of that used for Step 2 (Bloch analysis); (b) Deformed configuration ($\epsilon = 0.9$): oblique and top views of the unit cell as obtained from Step 1 (static analysis) and of that used for Step 2 (Bloch analysis); (c) corresponding point lattice in reciprocal space showing the *first Brillioun zone* (the area inside the yellow square) and the *irreducible Brillioun zone* (red GXM triangle) for square arrangement of helices. $\mathbf{b}_1$ and $\mathbf{b}_2$ are the reciprocal lattice vectors.

where p is the acoustic pressure, $\mathbf{x}$ is the position of a node in the deformed configuration and $\mathbf{r}$ denotes the distance in the current configuration between a pair of nodes periodically located on the boundary. Moreover, $\mathbf{k}$ is the Bloch-wave vector lying in the reciprocal space. Since most commercial finite element packages do not support the complex-valued pressure introduced by (S18), following Aberg and Gudmundson [2] we split any complex-valued spatial function $\phi(\mathbf{x})$ into a real and an imaginary part

$$\phi(\mathbf{x}) = \phi(\mathbf{x})^{re} + i\phi(\mathbf{x})^{im}. \tag{S19}$$

The problem is then solved using two identical finite element meshes for the unit cell, one for the real part and the other for the imaginary part, coupled by

$$\begin{aligned} \mathrm{p}^{re}(\mathbf{x}+\mathbf{r}) &= \mathrm{p}^{re}(\mathbf{x})\cos(\mathbf{k}\cdot\mathbf{r}) - \mathrm{p}^{im}(\mathbf{x})\sin(\mathbf{k}\cdot\mathbf{r}), \\ \mathrm{p}^{im}(\mathbf{x}+\mathbf{r}) &= \mathrm{p}^{re}(\mathbf{x})\sin(\mathbf{k}\cdot\mathbf{r}) + \mathrm{p}^{im}(\mathbf{x})\cos(\mathbf{k}\cdot\mathbf{r}). \end{aligned} \tag{S20}$$

Operationally, in our numerical simulations we use a user defined multiple point constraint (MPC) subroutine to implement Eqs. (S20).

Finally, focusing on the propagation of small-amplitude waves, we solve the frequency-domain acoustic wave equation [3]

$$\nabla \cdot (\frac{1}{\rho}\nabla \mathrm{p}) = -\frac{1}{\rho c_L^2}(\omega(\mathbf{k}))^2 \mathrm{p}, \tag{S21}$$

using a perturbation method to obtain the dispersion relations $\omega = \omega(\mathbf{k})$. Note that, since the reciprocal lattice is also periodic, we can restrict the wave vectors $\mathbf{k}$ to a certain region of the reciprocal space called the *first Brillioun zone* [4](indicated by the yellow square in Figure S4(c)). In addition, we may further reduce the domain to the *irreducible Brillioun zone*

(IBZ) (red triangle GXM in Figure S4(c)) by taking advantage of reflectional and rotational symmetries [3]. Operationally, the band gaps are identified by checking all the eigen-frequencies $\omega(\mathbf{k})$ for $\mathbf{k}$ vectors on the perimeter of the IBZ. The band gaps, defined as frequencies range in which the propagation of the waves is forbidden, are obtained by the frequency ranges within no $\omega(\mathbf{k})$ exist. Numerically, a discrete set of $\mathbf{k}$ vectors on the perimeter of the IBZ needs to be chosen for the band gap calculations. For the simulations presented in this paper, twenty uniformly-spaced points on each edge of the IBZ are considered.

Finally, we note that, given the large contrast in material properties between rubber and air, dispersion relations identical to those shown in the paper are obtained also for simplified models in which the elastomeric helix is modeled as a cavity and perfectly-reflecting boundary conditions are assumed at the interface (see Figure S5).

S5 Additional Results

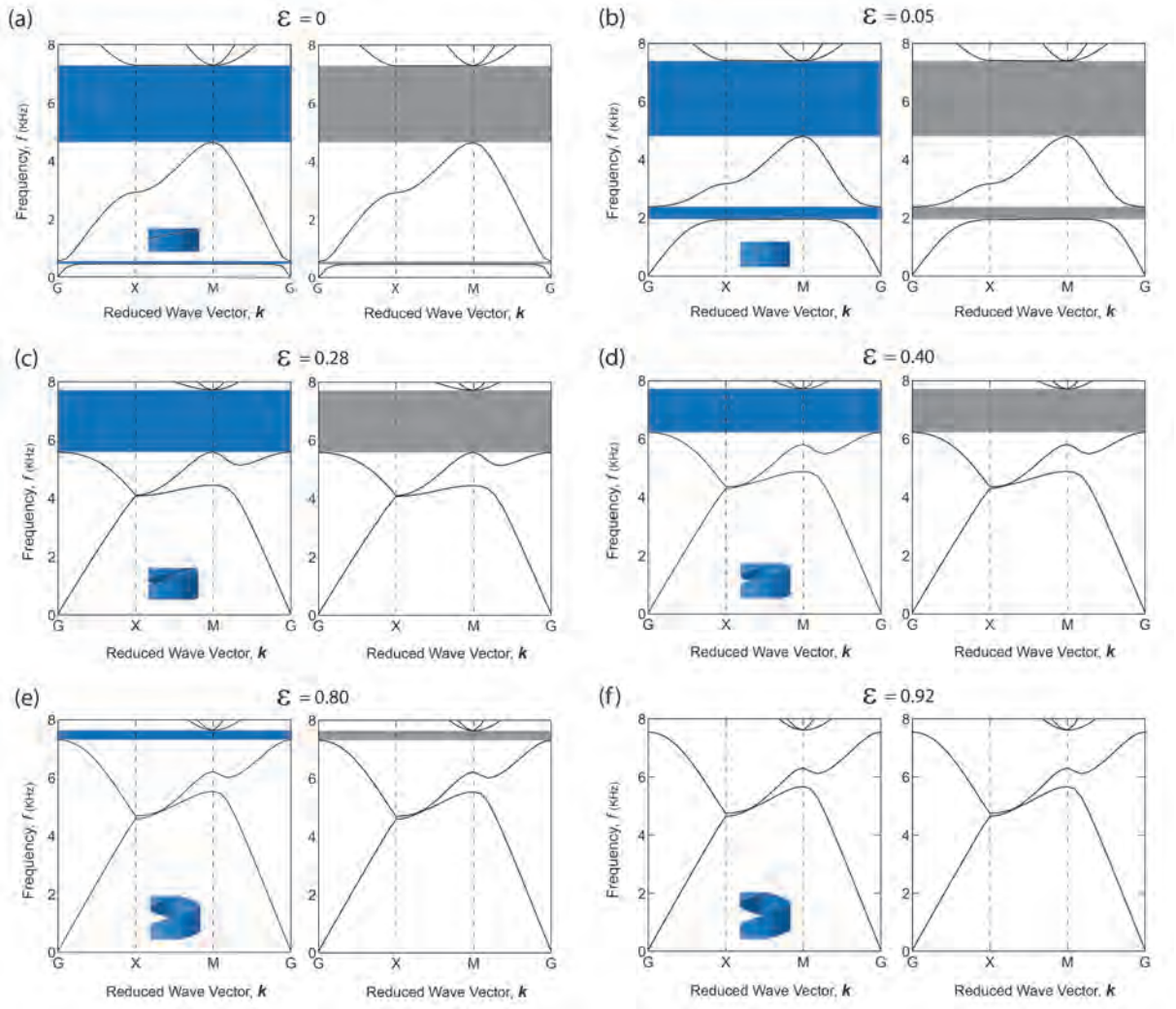

Figure S5: **Effect of the applied deformation on the dispersion relations for the fabricated structure.** Dispersion relations calculated at different levels of applied deformation. At each level of deformation the dispersion plots on the left (in blue) are obtained from models that comprise both the elastomeric helix and the surrounding air, while the dispersion plots on the right (in grey) are obtained from simplified models in which the elastomeric helix is modeled as a cavity and perfectly-reflecting boundary conditions are assumed at the interface. The results are reported at different levels of strains (a) $\epsilon = 0$, (b) $\epsilon = 0.05$, (c) $\epsilon = 0.28$, (d) $\epsilon = 0.40$, (e) $\epsilon = 0.80$, and (f) $\epsilon = 0.92$ under uniaxial tension. The insets show the configuration of helices at the corresponding levels of applied strains. The metamaterial comprises a square array of helices with initial outer diameter $D_0 = 28.6\ mm$, pitch $P_0 = 13\ mm$, rectangular cross-section of $13 \times 6.5\ mm$, and lattice spacing $A_0 = 32.5\ mm$.

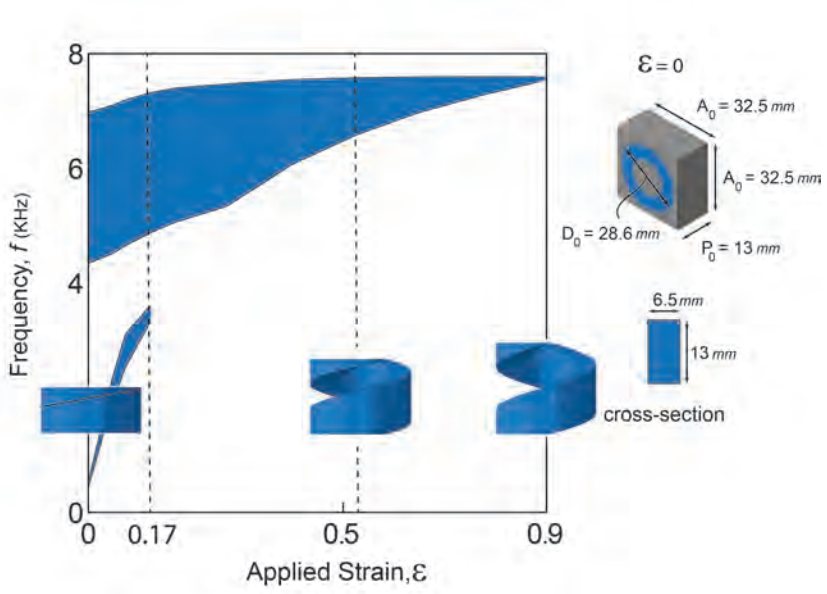

Figure S6: **Evolution of band gap frequency as a function of the applied deformation for the fabricated structure.** The metamaterial comprises a square array of helices with initial outer diameter $D_0 = 28.6\ mm$, pitch $P_0 = 13\ mm$, rectangular cross-section of $13 \times 6.5\ mm$, and lattice spacing $A_0 = 32.5\ mm$.

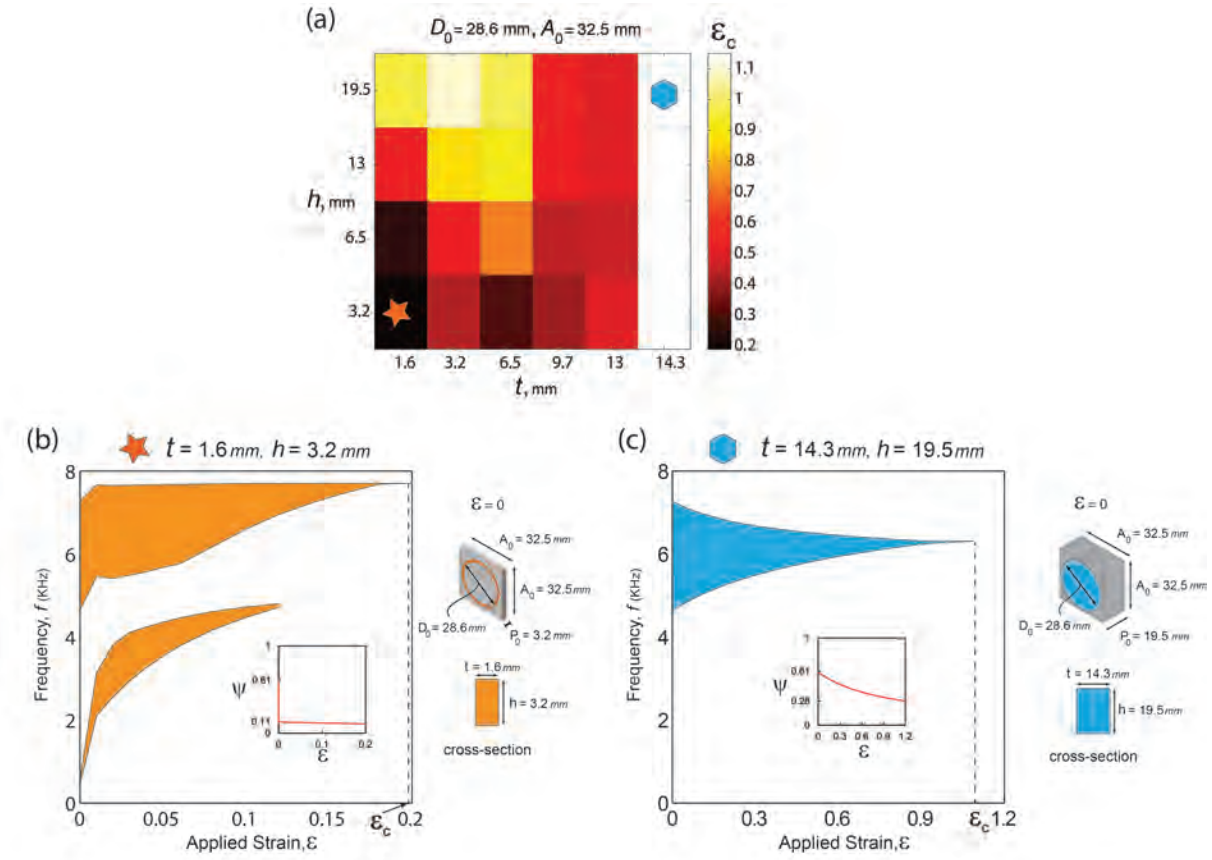

Figure S7: **Effect of the helix geometry on the the dynamic response of the metamaterial**. (a) Effect of the cross section dimensions $h = P_0$ and $t = (D_0 - D_{0,in})/2$ on the amount of strain needed to fully suppress the band gaps (ε_c) for a square array of helices with fixed initial outer diameter $D_0 = 28.6\ mm$ and lattice spacing $A_0 = 32.5\ mm$. The orange star and blue hexagon markers indicate configurations characterized by the lowest and highest values of ε_c, respectively. (b, c) Evolution of band gap frequency as a function of the applied deformation for the two configurations characterized by the lowest and highest values of ε_c. These two designs are defined by (b) $t = 1.6\ mm$ and $h = 3.2\ mm$, and (c) $t = 14.3\ mm$ and $h = 19.5\ mm$, both with initial outer diameter $D_0 = 28.6\ mm$ and lattice spacing $A_0 = 32.5\ mm$. The insets show the evolution of the solid volume fraction as function of the applied strain.

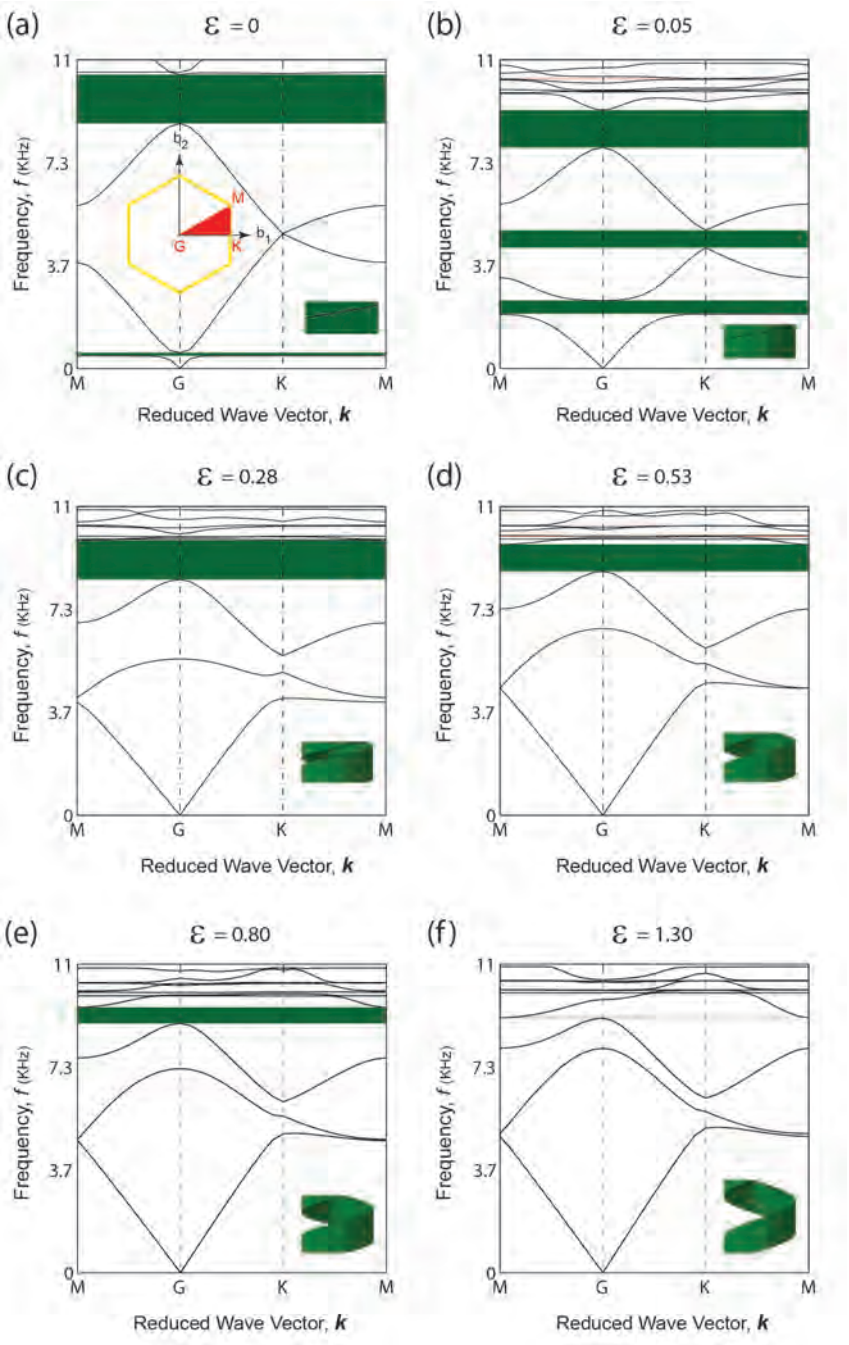

Figure S8: **Effect of the applied deformation on the dispersion relations of a triangular array of helices.** Dispersion relations calculated at different levels of applied deformation. The results are reported at different levels of strains (a) $\epsilon = 0$, (b) $\epsilon = 0.05$, (c) $\epsilon = 0.28$, (d) $\epsilon = 0.53$, (e) $\epsilon = 0.80$, and (f) $\epsilon = 1.30$ under uniaxial tension. The insets show the configuration of helices at the corresponding levels of applied strains. The metamaterial comprises a triangular array of helices with initial outer diameter $D_0 = 28.6\ mm$, pitch $P_0 = 13\ mm$, rectangular cross-section of $13 \times 6.5\ mm$, and lattice spacing $A_0 = 32.5\ mm$.

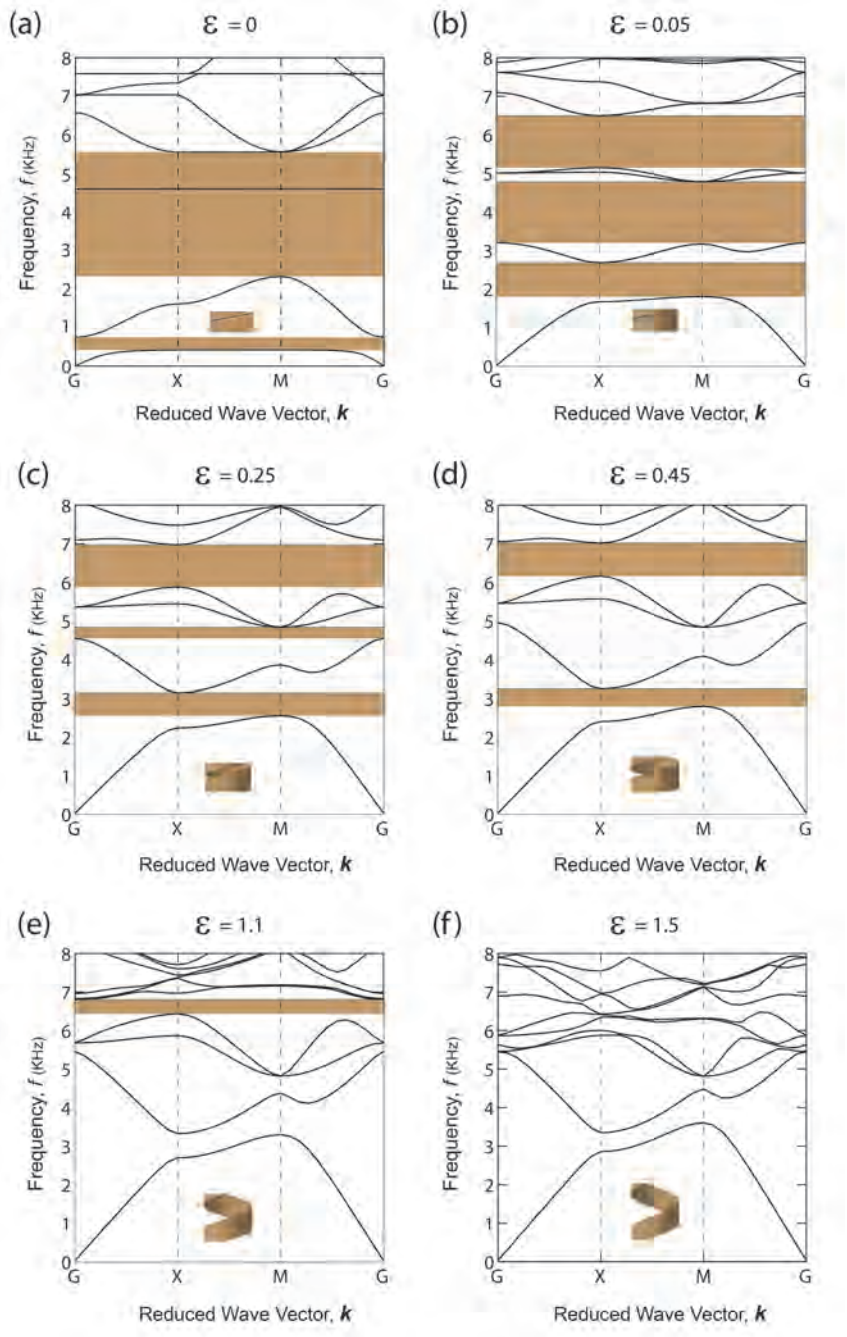

Figure S9: **Effect of the applied deformation on the dispersion relations of a square array of helices.** Dispersion relations calculated at different levels of applied deformation. The results are reported at different levels of strains (a) $\epsilon = 0$, (b) $\epsilon = 0.05$, (c) $\epsilon = 0.25$, (d) $\epsilon = 0.45$, (e) $\epsilon = 1.1$, and (f) $\epsilon = 1.5$ under uniaxial tension. The insets show the configuration of helices at the corresponding levels of applied strains. The metamaterial comprises a square array of helices with initial outer diameter $D_0 = 48\ mm$, pitch $P_0 = 24\ mm$, rectangular cross-section of $24 \times 2\ mm$, and lattice spacing $A_0 = 50\ mm$.

References

[1] Yeoh O (1993) Some forms of the strain energy function for rubber. *Rubber Chem. Technol.* 66:754–771.

[2] Aberg M, Gudmundson P (1997) The usage of standard finite element codes for computation of dispersion relations in materials with periodic microstructure. *The Journal of the Acoustical Society of America* 102:2007–2013.

[3] Maldovan M, Thomas EL (2009) *Periodic Materials and Interference Lithography: for Photonics, Phononics and Mechanics* (Wiley-VCH Verlag GmbH and Co. KGaA).

[4] Brillouin L (1946) *Wave Propagation in Periodic Structures* (McGraw-Hill).